Article

Ab Initio Kinetics of Electrochemical Reactions Using the Computational Fc^0/Fc^+ Electrode

Aleksandr S. Kramarenko, Dmitry I. Sharapa, Evgeny A. Pidko, and Felix Studt*

ACCESS | 📊 Metrics & More | 📖 Article Recommendations | 🔵SI Supporting Information

ABSTRACT: The current state-of-the-art electron-transfer modeling primarily focuses on the kinetics of charge transfer between an electroactive species and an inert electrode. Experimental studies have revealed that the existing Butler−Volmer model fails to satisfactorily replicate experimental voltammetry results for both solution-based and surface-bound redox couples. Consequently, experimentalists lack an accurate tool for predicting electron-transfer kinetics. In response to this challenge, we developed a density functional theory-based approach for accurately predicting current peak potentials by using the Marcus−Hush model. Through extensive cyclic voltammetry simulations, we conducted a thorough exploration that offers valuable insights for conducting well-informed studies in the field of electrochemistry.
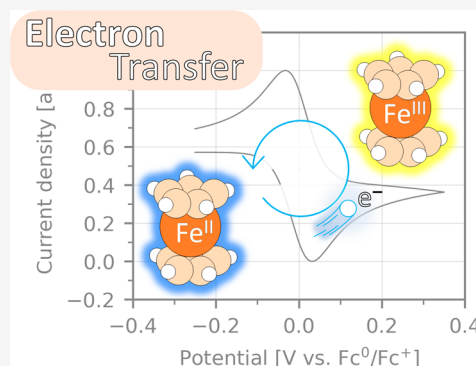
INTRODUCTION

Electron transfer kinetics plays a pivotal role in oxidation and reduction reactions, which are essential phenomena across various scientific disciplines including biology, physics, and chemistry. In physical chemistry, discussion about these processes and their kinetics primarily focus on the energy barriers of the elementary reaction steps.[1−9] In electrochemistry, these charge-transfer barriers, together with the diffusion of substrates and products to and from the electrode surface, determine the reaction kinetics and thus the form of the cyclic voltammogram, where the electric current is measured as a function of applied potential.[10]

The use of theoretical methods to calculate cyclic voltammograms is complicated by the fact that the barriers change as a function of the potential at the solid−liquid interface. Many studies have been devoted to simulate the full complexity of chemical transformations at the solid−liquid interface,[1,9,11−14] with the solid being an electrocatalyst that binds intermediates and influences[15−17] electrochemical reaction barriers.[3,12,14,18−22] However, recent works show that the first solvation layer of the electrode surface is mainly occupied by solvent molecules and supporting electrolyte ions which hinder direct interaction of electrochemically active species to the electrode surface.[22−26] Herein, we focus on identifying simple concepts to describe direct electron transfer from the electrode (cathode or anode) into the electrolyte (outer Helmholtz layer) without the explicit adsorption of intermediates on the electrode surface. We propose that this can be achieved by combining density functional theory (DFT) calculations with symmetric Marcus−Hush theory.[27−30] This nonempirical strategy allows accurate

prediction of standard reduction potentials and voltammetric features such as peak potentials and peak current. The method is validated by computing reduction potentials and activation barriers of an extensive list of organic molecules (Figure S1), that have been discussed for a broad range of applications such as for energy storage,[31−34] dyes,[35−37] and photoresponsive membrane production.[33,38−41]
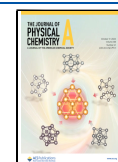
METHODS

We start by investigating the performance of popular DFT methods in predicting the thermodynamics of electrochemical reactions. Structures of all chemical species employed in this study were fully relaxed using an unrestricted Kohn−Sham approach. We considered a representative selection of popular exchange−correlation functionals (BHANHLYP, B3LYP, BLYP, M06-2X, M06, M06-L, PBE, and PBE0) together with the ma-def2-TZVPP basis set as implemented in the ORCA (version 5.0.3) code.[42−44] Our starting point is the redox couple ferrocene−ferrocenium (Fc^0/Fc^+) that is widely applied as a reference system in electrochemical reactions.[4,45−64] Solvation effects of acetonitrile (MeCN), dimethylformamide (DMF), and acetone (ACE) have been taken into account by using the CPCM solvation model[65] implemented in ORCA. A detailed description of the

computational methodology is given in the Supporting Information (SI).

RESULTS AND DISCUSSION

We benchmark the various functionals for the (Fc^0/Fc^+) redox couple using the absolute electrode potential (AEP) of the reference electrode as described by eq 1.

$$AEP_{calc} = G_{red} - G_{ox} \tag{1}$$

where G_{red} is the Gibbs free energy of the corresponding Fc^0 state and G_{ox} is the free energy of the Fc^+ cation radical. As the Fc^0/Fc^+ system is a well-known reference due to its wide applicability in electrochemistry, there are plethora of experimental ionization potentials obtained by photoelectron and/or electron impact spectroscopy.[4,59] In our current study, we rely on the experimental value of 6.71 ± 0.08 eV for its gas-phase ionization energy reported by the National Institute of Standards and Technology (NIST).[59] The gas-phase ionization energies for all examined functionals are summarized in Figure S2 and elaborated upon in detail in the Supporting Information. Briefly, both the M06[66] and PBE[67,68] functionals perform best, with values of 6.76 and 6.78 eV, respectively. The accuracy of the studied functionals is influenced by spin contamination, which negatively impacts the Hartree−Fock methods more significantly than the DFT methods. As a result, a higher Hartree−Fock exchange component within the functional leads to an increased incidence of spin contamination. It has been shown that the ferrocenium cation can be affected by this issue in both DLPNO−CCSD(T)[69] and double-hybrid calculations.[70]

Experimentally, AEPs in solution are usually measured against reference electrodes and calculated according to

$$AEP_{solv} = (E^0 + E_{ref})nF \tag{2}$$

where AEP_{solv} denotes the AEP in a specific solvent, F is the Faraday constant, E_{ref} is the absolute potential of the reference electrode in a particular solvent, n denotes the number of electrons transferred during the process, and E^0 corresponds to the experimental standard reduction potential. The AEP_{solv} values for several most often used aprotic solvents are summarized in Table 1 and compared to our computational results using the PBE and M06 functionals (all other functionals have worse performance, see the Supporting Information).
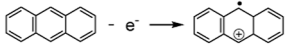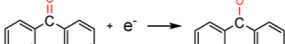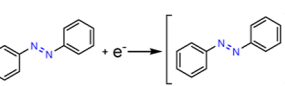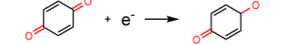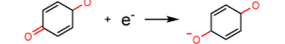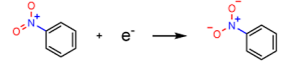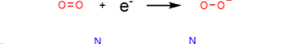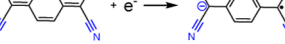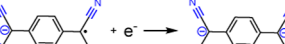
Table 1. Comparison of Experimental and Computed AEPs in Solution (AEP_{solv}) of the Fc^0/Fc^+ System in MeCN, DMF, and ACE Solvents

solvent	AEP_{solv} [eV]		
	experiment	calculations	
		PBE	M06
MeCN	4.88,[2,13] 4.90,[71] 5.25[55]	5.26	4.85
DMF	5.33,[64,72] 4.72[73,74]	5.28	5.03
ACE	5.46,[48,53] 4.74[75]	5.61	6.90

As can be seen from Table 1, both functionals give reasonable results, especially considering that there is also large disagreement among the experimentally reported data.[55,59,61] In this study, we are interested in the absolute potential of Fc^0/Fc^+ in an acetonitrile solution, where the average value of the experimentally obtained absolute

potentials is 5.01 eV with a mean absolute error (MAE) of 0.16 eV.

We will use this computational Fc^0/Fc^+ electrode (CFE) to investigate the electroreduction of a test set of 13 different reactions (Figure 1). Figure 2 presents the results obtained

#	Reactions	E^0 [V vs. Fc^+/Fc^0]
1		0.84
2		-2.34
3		-1.86
4		-1.00
5		-1.86
6		-1.61
7		-1.28
8		-0.33
9		-0.75
10		0.77
11		1.28
12		-0.16
13		0.20

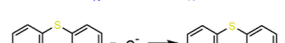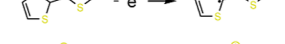**Figure 1.** Reference reactions used for estimation of reduction potential prediction accuracy and its experimental standard reduction potentials were extracted from the published literature.

with the M06 functional, while the respective data obtained with the PBE and other DFT methods are summarized in the Supporting Information.

The error bars in Figure 2 represent the deviation of experimentally observed reduction potentials due to the error raised from the reference system. Figure 2 confirms the high accuracy of our computational Fc^0/Fc^+ electrode at the M06 level for the estimation of the reduction potentials of this test set with a mean absolute error of only 0.18 V. Note that this error is within the accuracy of typical DFT functionals (±0.20 eV). Note that the experiments also deviate in reported reduction potentials, with deviations between experiments being as large as 0.16 V. Having established that we are able to calculate SRPs and thus the thermodynamics of an electrochemical system using the CFE, we will now use this to evaluate electron-transfer kinetics in the framework of the Marcus−Hush model.[27,28,76−81] According to Marcus−Hush theory, the activation energy ($G_f^{\ddagger}$ and $G_b^{\ddagger}$ for the forward and
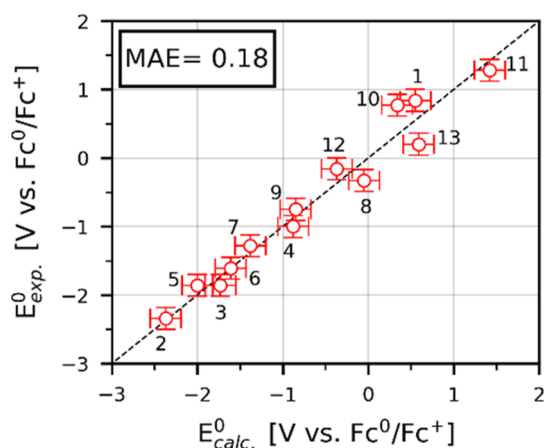
Figure 2. Comparison of experimental and calculated reduction potentials of the test set of 13 reactions from Figure 1 using CFE with the M06 functional.

backward reactions, respectively) of an electron-transfer process can be calculated by

$$G_f^{\ddagger} = \frac{\lambda}{4} + \alpha F(E - E^0) \tag{3}$$

$$G_b^{\ddagger} = \frac{\lambda}{4} - (1 - \alpha)F(E - E^0) \tag{4}$$

where λ is the reorganization energy[82] and α is a potential-dependent symmetry factor. This parameter can be evaluated by the following equation

$$\alpha = \frac{1}{2} + \frac{F(E - E^0)}{4\lambda} \tag{5}$$

λ consists of the inner (λ_i) and outer sphere (λ_o) reorganization energy and is

$$\lambda = \lambda_i + \lambda_o \tag{6}$$

In the given equation, λ_i represents the reorganization energy associated with alterations in bond lengths and angles between atoms during the electron-transfer process, which can rather be simply obtained from DFT calculations. For the forward reaction barrier ($G_f^{\ddagger}$), this is done by calculating the differences of free energy of the reduced state with the equilibrium geometry of the oxidized (Q_{ox}) and reduced states (Q_{red}). In the case of Fc^0/Fc$^+$ system $G_{red}(Q_{ox})$ equals to free energy of ferrocene in optimized ferrocenium geometry and $G_{red}(Q_{red})$ is the free energy of ferrocene with relaxed ferrocene geometry.

$$\lambda_i = G_{red}(Q_{ox}) - G_{red}(Q_{red}) \tag{7}$$

λ_o can be calculated from

$$\lambda_o = \frac{e^2}{8\pi\varepsilon_0}\left(\frac{1}{a_o} - \frac{1}{R}\right)\left(\frac{1}{\varepsilon_{op}} - \frac{1}{\varepsilon_s}\right) \tag{8}$$

where e is the elementary charge, ε_0 is the vacuum dielectric permittivity, while a_0 signifies the radius of a sphere of the corresponding molecule the volume of which is equivalent to the cavity volume in the solvation model, ε_{op} and ε_s are optical and static dielectric permittivity, R is a distance of the molecule from the electrode surface and usually equals to $2a_0$.

Applying this for our case of the Fc^0/Fc$^+$ system, λ is equal to 0.30 eV, with λ_i being calculated to 0.02 eV by DFT and λ_o being 0.28 eV. We computed the activation energy for both the forward and backward reactions of the Fc^0/Fc$^+$ redox couple using eqs 3 and 4, and the result is depicted in Figure 3.
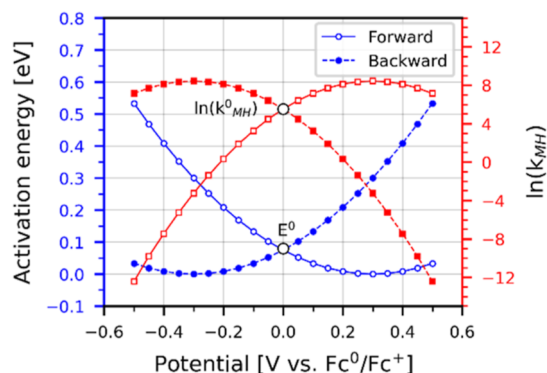
Figure 3. Dependence of the activation energy (dots) and rate constants (squares) for the Fc^0/Fc$^+$ oxidation process on the applied potential. The white circles at 0 V correspond to the respective values at the standard reduction potential.

Having derived the expression for the activation energies for electron transfer as a function of applied potential, one can now compute the potential-dependent rate constants for the forward and backward reactions

$$k_f = k^0 e^{-\alpha F(E - E^0)/RT} \tag{9}$$

$$k_b = k^0 e^{(1-\alpha)F(E - E^0)/RT} \tag{10}$$

where k^0 is the standard rate constant, which is dependent on the total reorganization energy λ. This parameter can be calculated from the following equation

$$k^0 = Ze^{-\lambda F/4RT} \tag{11}$$

$$Z = \sqrt{\frac{RT}{2\pi M}} \tag{12}$$

where Z is the collision frequency with the electrode surface which depends on the molar mass (M) of the molecule.

The reaction rate also depends crucially on the concentration of the molecules in the volume above the electrode surface. The concentration is dependent on the conversion and diffusion of molecules during electroreduction and oxidation. The reaction rate (and thus the current density) is thus given by eqs 13 and 14

$$\frac{dC_i}{dt} = D_i \frac{d^2C_i}{dt^2} \tag{13}$$

$$-J_{ox} = J_{red} = k_f C_A - k_b C_B \tag{14}$$

where k_f and k_b are rate constants computed by the Marcus–Hush model, C_A and C_B represent the concentration of Fc^0 and Fc$^+$, respectively, and D_i is the diffusion constant of a solute.

Final current density can be calculated from eq 15

$$\frac{i_{tot}}{A} = -nFJ_{ox} \tag{15}$$

where n is the number of transferred electrons, F is Faraday's constant, A is the surface area of the electrode, and i_{tot} is the

reaction current; eqs 13−15 were computed numerically using the finite difference method.[77,84,85] A detailed procedure of cyclic voltammetry (CV) simulation was described by Brown.[86] Python code used for CV curve production can be found on KITopen.

We computed the diffusion constant (D_i) using the Einstein−Stokes equation

$$D_i = \frac{k_b T}{6\pi\eta a_i} \tag{16}$$

where k_b is the Boltzmann constant and η is the solvent viscosity. The viscosity of acetonitrile at 298.15 K equals to 0.38 mPa·s.[60] Thus, the calculated diffusion coefficients are 0.954×10^{-5} and 0.951×10^{-5} cm^2/s for Fc^0 and Fc$^+$, respectively. This fits well with experimentally obtained values of 2.00×10^{-5} and 1.60×10^{-5} cm^2/s for Fc^0 and Fc$^+$, respectively.[46]

Using eqs 13 and 14, we simulated the CV curves of Fc^0/Fc$^+$. The simulated and experimental[83] CV curves are compared in Figure 4. Concentrations of all components of
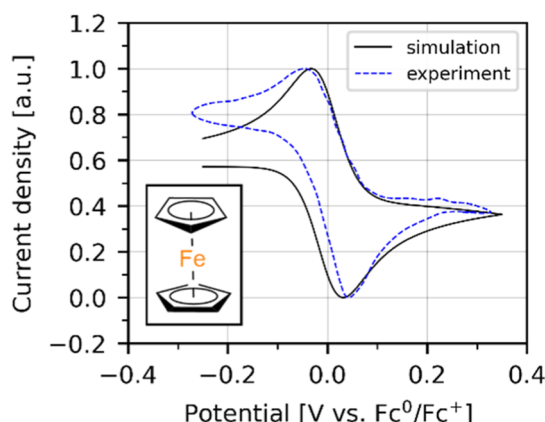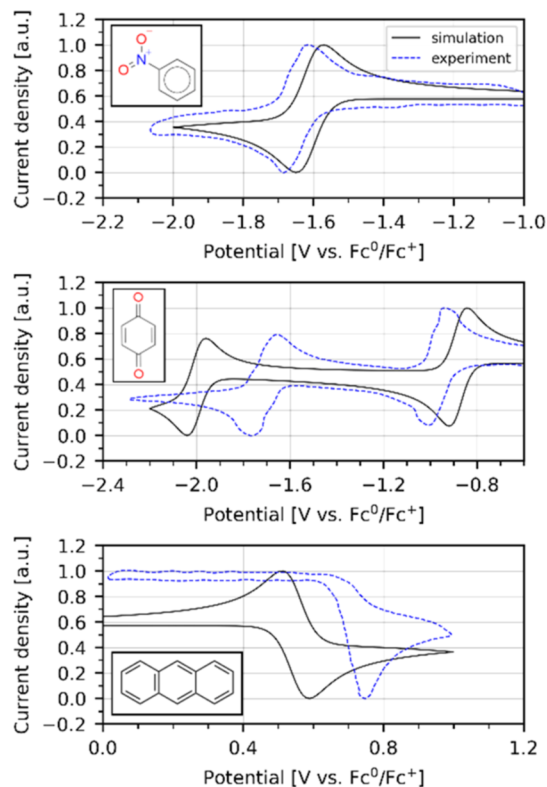

Figure 4. Experimental and simulated CV curves of 5 mM ferrocene oxidation at a 0.01 V/s scan rate. Solid line represents the simulated CV curve and dashed line represents the experimental CV curve. The provided values represent simulated/experimental peak potentials and standard reduction potentials. The experimental CV curve is adapted from ref 83. Available under a CC-BY 3.0 license. Copyright 2024 K. Lehmann, O. Yurchenko and G. Urban.

the reaction medium in the simulations were set to reproduce the experimental conditions. In the simulation of ferrocene behavior, where reduction potential were established at 0 V vs Fc^0/Fc$^+$, the positions of peak potentials exhibit slight variations compared to the experimental results with the peak potential difference being 0.06 V for our simulation and 0.08 V for experimental results.[83] We can thus nicely simulate the CV curves of our computational Fc^0/Fc$^+$ electrode using exclusive input from DFT calculations as well as the tabulated viscosity of acetonitrile as the input.

We now turn to simulate the CV curves of the 13 test reactions depicted in Figure 1. We do this in the same manner and use our computational Fc^0/Fc$^+$ electrode as the reference electrode, as was done in Figure 2 (the solvent being acetonitrile in all cases). The results are shown in Figure 5 for a selected set of reactions (see the Supporting Information for the CV curves of all 13 reactions).

Experimental CV curves from Figure 5 were adapted from published experiments.[39,54] In all cases shown in Figure 5,


Figure 5. Experimental and simulated CV curves of nitrobenzene, benzoquinone reduction, and anthracene oxidation with 0.1, 0.1, and 0.1 V/s scan rate, respectively. Solid line represents the simulated CV curve and dashed line represents the experimental CV curves (see text). Experimental CV curves for nitrobenzene adapted with permission from ref 39. Copyright 2024 Royal Society of Chemistry. Experimental CV curves for benzoquinone and anthracene are adapted with permission from refs 38 and 41. Copyright 2024 Elsevier.

deviation from experimentally observed reaction behavior can be explained by the difference in experimental[39,77,87,88] and predicted reduction potentials. However, experimental anthracene oxidation does not show a cathodic peak from cation radical deactivation which was observed for anthracene derivatives on the Pt electrode.[89] It might be related to the chemical step, which was not considered in the current study. This process was shown to be a fast step,[90] hence the reversed process of An$^+$ reduction is hindered due to lack of cation radicals.[91]

Furthermore, by comparing the experimental peak potentials to the simulated values, we can evaluate the reproduction of kinetic parameters. We also stress here that the discrepancies are mostly due to errors originating from inaccuracies of the DFT functional, as an error of, e.g., 0.2 eV translates directly to a deviation of 0.2 V in the simulated CV.

Figure 6 illustrates a comparison between the experimental and simulated peak potentials for investigated test reactions in which experimental CVs have been found. The analysis indicates that the predicted peak potentials align well with the experimental results, within the typical error introduced by DFT. The mean average deviation for the model was estimated to be 0.33 V vs Fc^0/Fc$^+$. Significant deviations from experimental results were primarily observed, when computational errors in reduction potentials existed.
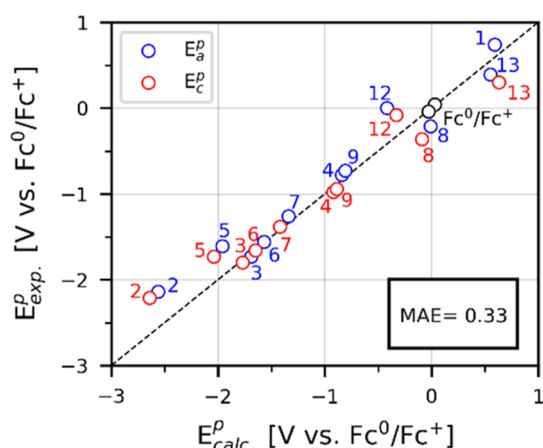
Figure 6. Representation of accuracy for peak potential prediction by the Marcus−Hush model. E_a^p and E_c^p are anodic and cathodic peak potentials, respectively. Numbers denote the reaction indexes in Figure 1.

CONCLUSIONS

In conclusion, our study explores the development of a straightforward ab initio model for predicting electrochemical kinetics and constructing CV curves of the 13 reference reactions and the ferrocene/ferrocenium system in particular. Moving beyond potential energies, our investigation extended to the electrode reaction kinetics. Utilizing the Marcus−Hush model, we obtained activation energies for reference reactions, shedding light on the electron-transfer process. The M06 functional stood out as providing the most accurate predictions for reduction potentials and facilitating precise calculations of activation energies. Furthermore, our computational approach can be broadened to account for the electrode electronic structure[81,92,93] with advanced models of reorganization energy calculation[78,79,82,94,95] to study electron transfer on various materials.

Furthermore, the study employed CV simulations to gain insights into the electrochemical behavior. We introduce here the computational Fc^0/Fc^+ electrode as a convenient reference electrode in computational studies and suggest that this can be universally employed as a reference for electron-transfer processes analogous to the computational hydrogen electrode that has been shown to work well for coupled proton-/ electron-transfer processes. The model, validated against experimental data, showcased its utility in predicting peak potentials and current density responses. While deviations were observed, particularly in reduction potentials impacting peak potentials, the model provided a qualitative representation of the electrochemical processes.

ASSOCIATED CONTENT

Data Availability Statement

Python code for CV simulations can be found via https://doi.org/10.35097/VKVYEoWBRxzhwiPh.

Ⓢ Supporting Information

The Supporting Information is available free of charge at https://pubs.acs.org/doi/10.1021/acs.jpca.4c04923.

> Optimized structures of all molecules utilized in this study, experimental and computed reduction potentials, and all data points utilized for constructing figures (PDF)

AUTHOR INFORMATION

Corresponding Author

Felix Studt − *Institute of Catalysis Research and Technology, Karlsruhe Institute of Technology, 76344 Eggenstein-Leopoldshafen, Germany; Institute for Chemical Technology and Polymer Chemistry, Karlsruhe Institute of Technology, 76131 Karlsruhe, Germany;* ⓞ orcid.org/0000-0001-6841-4232; Email: felix.studt@kit.edu

Authors

Aleksandr S. Kramarenko − *Institute of Catalysis Research and Technology, Karlsruhe Institute of Technology, 76344 Eggenstein-Leopoldshafen, Germany*

Dmitry I. Sharapa − *Institute of Catalysis Research and Technology, Karlsruhe Institute of Technology, 76344 Eggenstein-Leopoldshafen, Germany;* ⓞ orcid.org/0000-0001-9510-9081

Evgeny A. Pidko − *Inorganic Systems Engineering Group, Department of Chemical Engineering, Faculty of Applied Sciences, Delft University of Technology, Delft 2628 CN, The Netherlands;* ⓞ orcid.org/0000-0001-9242-9901

Complete contact information is available at:
https://pubs.acs.org/10.1021/acs.jpca.4c04923

Author Contributions

The manuscript was written through contributions of all authors. All authors have given approval to the final version of the manuscript.

Notes

The authors declare no competing financial interest.

REFERENCES

(1) Goodpaster, J. D.; Bell, A. T.; Head-Gordon, M. Identification of Possible Pathways for C-C Bond Formation during Electrochemical Reduction of CO2: New Theoretical Insights from an Improved Electrochemical Model. *J. Phys. Chem. Lett.* **2016**, 7 (8), 1471−1477.

(2) Isse, A. A.; Lin, C. Y.; Coote, M. L.; Gennaro, A. Estimation of Standard Reduction Potentials of Halogen Atoms and Alkyl Halides. *J. Phys. Chem. B* **2011**, 115 (4), 678−684.

(3) Valdés, Á.; Qu, Z.-W.; Kroes, G.-J.; Rossmeisl, J.; Nørskov, J. K. Oxidation and Photo-Oxidation of Water on TiO2 Surface. *J. Phys. Chem. C* **2008**, 112 (26), 9872−9879.

(4) Toma, M.; Kuvek, T.; Vrček, V. Ionization Energy and Reduction Potential in Ferrocene Derivatives: Comparison of Hybrid and Pure DFT Functionals. *J. Phys. Chem. A* **2020**, 124 (39), 8029−8039.

(5) Steinmann, S. N.; Michel, C.; Schwiedernoch, R.; Sautet, P. Impacts of Electrode Potentials and Solvents on the Electroreduction of CO2: A Comparison of Theoretical Approaches. *Phys. Chem. Chem. Phys.* **2015**, 17 (21), 13949−13963.

(6) Gutiérrez-Sánchez, O.; de Mot, B.; Daems, N.; Bulut, M.; Vaes, J.; Pant, D.; Breugelmans, T. Electrochemical Conversion of CO2 from Direct Air Capture Solutions. *Energy Fuels* **2022**, 36 (21), 13115−13123.

(7) Billy, J. T.; Co, A. C. Experimental Parameters Influencing Hydrocarbon Selectivity during the Electrochemical Conversion of CO2. *ACS Catal.* **2017**, *7* (12), 8467−8479.

(8) Li, J.; Tian, X.; Wang, X.; Zhang, T.; Spadaro, M. C.; Arbiol, J.; Li, L.; Zuo, Y.; Cabot, A. Electrochemical Conversion of Alcohols into Acidic Commodities on Nickel Sulfide Nanoparticles. *Inorg. Chem.* **2022**, *61* (34), 13433−13441.

(9) Huang, Y.-F.; Wu, D.-Y.; Wang, A.; Ren, B.; Rondinini, S.; Tian, Z.-Q.; Amatore, C. Bridging the Gap between Electrochemical and Organometallic Activation: Benzyl Chloride Reduction at Silver Cathodes. *J. Am. Chem. Soc.* **2010**, *132* (48), 17199−17210.

(10) Beinlich, S. D.; Kastlunger, G.; Reuter, K.; Hörmann, N. G. Controlled Electrochemical Barrier Calculations without Potential Control. *J. Chem. Theory Comput.* **2023**, *19* (22), 8323−8331.

(11) Cheng, T.; Xiao, H.; Goddard, W. A. Free-Energy Barriers and Reaction Mechanisms for the Electrochemical Reduction of CO on the Cu(100) Surface, Including Multiple Layers of Explicit Solvent at pH 0. *J. Phys. Chem. Lett.* **2015**, *6* (23), 4767−4773.

(12) Nørskov, J. K.; Rossmeisl, J.; Logadottir, A.; Lindqvist, L.; Kitchin, J. R.; Bligaard, T.; Jónsson, H. Origin of the Overpotential for Oxygen Reduction at a Fuel-Cell Cathode. *J. Phys. Chem. B* **2004**, *108* (46), 17886−17892.

(13) Granda-Marulanda, L. P.; McCrum, I. T.; Koper, M. T. M. A Simple Method to Calculate Solution-Phase Free Energies of Charged Species in Computational Electrocatalysis. *J. Phys.: Condens. Matter* **2021**, *33* (20), 204001.

(14) Chen, L. D.; Urushihara, M.; Chan, K.; Nørskov, J. K. Electric Field Effects in Electrochemical CO2 Reduction. *ACS Catal.* **2016**, *6* (10), 7133−7139.

(15) Chaturvedi, A.; McCarver, G. A.; Sinha, S.; Hix, E. G.; Vogiatzis, K. D.; Jiang, J. A PEGylated Tin Porphyrin Complex for Electrocatalytic Proton Reduction: Mechanistic Insights into Main-Group-Element Catalysis. *Angew. Chem., Int. Ed.* **2022**, *61* (34), No. e202206325.

(16) Bairagi, A.; Pereverzev, A. Y.; Tinnemans, P.; Pidko, E. A.; Roithová, J. Electrocatalytic CO2 Reduction: Monitoring of Catalytically Active, Downgraded, and Upgraded Cobalt Complexes. *J. Am. Chem. Soc.* **2024**, *146* (8), 5480−5492.

(17) Zhang, L.-H.; Mathew, S.; Hessels, J.; Reek, J. N. H.; Yu, F. Homogeneous Catalysts Based on First-Row Transition-Metals for Electrochemical Water Oxidation. *ChemSusChem* **2021**, *14* (1), 234−250.

(18) Ludwig, T.; Gauthier, J. A.; Dickens, C. F.; Brown, K. S.; Ringe, S.; Chan, K.; Nørskov, J. K. Atomistic Insight into Cation Effects on Binding Energies in Cu-Catalyzed Carbon Dioxide Reduction. *J. Phys. Chem. C* **2020**, *124* (45), 24765−24775.

(19) Göttle, A. J.; Koper, M. T. M. Proton-Coupled Electron Transfer in the Electrocatalysis of CO2 Reduction: Prediction of Sequential vs. Concerted Pathways Using DFT. *Chem. Sci.* **2017**, *8* (1), 458−465.

(20) Zhao, H.; Lv, X.; Wang, Y.-G. Realistic Modeling of the Electrocatalytic Process at Complex Solid-Liquid Interface. *Advanced Science* **2023**, *10* (32), 2303677.

(21) Zhang, Z.; Wei, Z.; Sautet, P.; Alexandrova, A. N. Hydrogen-Induced Restructuring of a Cu(100) Electrode in Electroreduction Conditions. *J. Am. Chem. Soc.* **2022**, *144* (42), 19284−19293.

(22) Sinha, V.; Khramenkova, E.; Pidko, E. A. Solvent-Mediated Outer-Sphere CO2 Electro-Reduction Mechanism over the Ag111 Surface. *Chem. Sci.* **2022**, *13* (13), 3803−3808.

(23) Kramarenko, A. S.; Chernyshov, I. Yu.; Pidko, E. A. Electric Double Layer Effect on the Outer-Sphere Benzyl Halides Electro-Reduction Mechanism. *J. Phys. Chem. C* **2024**, *128* (23), 9462−9471.

(24) Kislenko, S. A.; Amirov, R. H.; Samoylov, I. S. Effect of Cations on the TiO2/Acetonitrile Interface Structure: A Molecular Dynamics Study. *J. Phys. Chem. C* **2013**, *117* (20), 10589−10596.

(25) Feng, G.; Huang, J.; Sumpter, B. G.; Meunier, V.; Qiao, R. Structure and Dynamics of Electrical Double Layers in Organic Electrolytes. *Phys. Chem. Chem. Phys.* **2010**, *12* (20), 5468−5479.

(26) Shin, S.-J.; Kim, D. H.; Bae, G.; Ringe, S.; Choi, H.; Lim, H.-K.; Choi, C. H.; Kim, H. On the Importance of the Electric Double Layer Structure in Aqueous Electrocatalysis. *Nat. Commun.* **2022**, *13* (1), 174.

(27) Rees, N. V.; Clegg, A. D.; Klymenko, O. V.; Coles, B. A.; Compton, R. G. Marcus Theory for Outer-Sphere Heterogeneous Electron Transfer: Predicting Electron-Transfer Rates for Quinones. *J. Phys. Chem. B* **2004**, *108* (34), 13047−13051.

(28) Andrieux, C. P.; Le Gorande, A.; Saveant, J. M. Electron Transfer and Bond Breaking. Examples of Passage from a Sequential to a Concerted Mechanism in the Electrochemical Reductive Cleavage of Arylmethyl Halides. *J. Am. Chem. Soc.* **1992**, *114* (17), 6892−6904.

(29) Savéant, J. M.; Tessier, D. Variation of the Electrochemical Transfer Coefficient with Potential. *Faraday Discuss. Chem. Soc.* **1982**, *74* (0), 57−72.

(30) Weaver, M. J. Correlations between Electrochemical and Homogeneous Redox Reactivity. Quantitative Comparisons of Rate Constants and Activation Parameters for Some Inorganic Outer-Sphere Reactions. *J. Phys. Chem.* **1980**, *84* (6), 568−576.

(31) Wang, X.; Chai, J.; Devi, N.; Lashgari, A.; Chaturvedi, A.; Jiang, "J." Two-electron-active tetracyanoethylene for nonaqueous redox flow batteries. *J. Mater. Chem. A* **2021**, *9* (24), 13867−13873.

(32) Daub, N.; Hendriks, K. H.; Janssen, R. A. J. Two-Electron Tetrathiafulvalene Catholytes for Nonaqueous Redox Flow Batteries. *Batteries Supercaps* **2022**, *5* (12), No. e202200386.

(33) Astudillo Sánchez, P. D.; Evans, D. H. Effect of Hydroxylic Additives on the Electrochemical Reduction of Some Azobenzenes. *J. Electroanal. Chem.* **2010**, *638* (1), 84−90.

(34) Chicas-Baños, D. F.; López-Rivas, M.; González-Bravo, F. J.; Sartillo-Piscil, F.; Frontana-Uribe, B. A. Access to Carbonyl Compounds *via* the Electroreduction of *N*-Benzyloxyphthalimides: Mechanism Confirmation and Preparative Applications. *Heliyon* **2024**, *10* (1), No. e23808.

(35) Atifi, A.; Ryan, M. D. Voltammetry and Spectroelectrochemistry of TCNQ in Acetonitrile/RTIL Mixtures. *Molecules* **2020**, *25* (2), 303.

(36) Harris, A. R.; Neufeld, A. K.; O'Mullane, A. P.; Bond, A. M.; Morrison, R. J. S. Voltammetric, EQCM, Spectroscopic, and Microscopic Studies on the Electrocrystallization of Semiconducting, Phase I, CuTCNQ on Carbon, Gold, and Platinum Electrodes by a Nucleation-Growth Process. *J. Electrochem. Soc.* **2005**, *152* (9), C577.

(37) Saiki, H.; Takami, K.; Tominaga, T. Diffusion of Porphyrins and Quinones in Organic Solvents. *Phys. Chem. Chem. Phys.* **1999**, *1* (2), 303−306.

(38) Mathieu-Scheers, E.; Bouden, S.; Grillot, C.; Nicolle, J.; Warmont, F.; Bertagna, V.; Cagnon, B.; Vautrin-Ul, C. Trace Anthracene Electrochemical Detection Based on Electropolymerized-Molecularly Imprinted Polypyrrole Modified Glassy Carbon Electrode. *J. Electroanal. Chem.* **2019**, *848*, 113253.

(39) Ohba, T.; Ishida, H.; Yamaguchi, T.; Horiuchi, T.; Ohkubo, K. Carbon Dioxide-Promoted Electrochemical Reduction of Aromatic Nitro Compounds to Azoxy Compounds in Acetonitrile. *J. Chem. Soc., Chem. Commun.* **1994**, 263−264.

(40) Tsierkezos, N. G. Investigation of the Electrochemical Reduction of Benzophenone in Aprotic Solvents Using the Method of Cyclic Voltammetry. *J. Solution Chem.* **2007**, *36* (10), 1301−1310.

(41) Astudillo, P. D.; Valencia, D. P.; González-Fuentes, M. A.; Díaz-Sánchez, B. R.; Frontana, C.; González, F. J. Electrochemical and Chemical Formation of a Low-Barrier Proton Transfer Complex between the Quinone Dianion and Hydroquinone. *Electrochim. Acta* **2012**, *81*, 197−204.

(42) Neese, F. The ORCA Program System. *WIREs Comput. Mol. Sci.* **2012**, *2* (1), 73−78.

(43) Neese, F. Software Update: The ORCA Program System—Version 5.0. *WIREs Comput. Mol. Sci.* **2022**, *12* (5), No. e1606.

(44) Neese, F.; Wennmohs, F.; Becker, U.; Riplinger, C. The ORCA Quantum Chemistry Program Package. *J. Chem. Phys.* **2020**, *152* (22), 224108.

(45) Yang, Y.; Yu, L. Theoretical Investigations of Ferrocene/Ferrocenium Solvation in Imidazolium-Based Room-Temperature Ionic Liquids. *Phys. Chem. Chem. Phys.* **2013**, *15* (8), 2669−2683.

(46) Wang, Y.; Rogers, E. I.; Compton, R. G. The Measurement of the Diffusion Coefficients of Ferrocene and Ferrocenium and Their Temperature Dependence in Acetonitrile Using Double Potential Step Microdisk Electrode Chronoamperometry. *J. Electroanal. Chem.* **2010**, *648* (1), 15−19.

(47) Warratz, R.; Aboulfadl, H.; Bally, T.; Tuczek, F. Electronic Structure and Absorption Spectra of Biferrocenyl and Bisfulvenide Diiron Radical Cations: Detection and Assignment of New Low-Energy Transitions. *Chem.-Eur. J.* **2009**, *15*, 1604−1617.

(48) Tsierkezos, N. G. Cyclic Voltammetric Studies of Ferrocene in Nonaqueous Solvents in the Temperature Range from 248.15 to 298.15 K. *J. Solution Chem.* **2007**, *36* (3), 289−302.

(49) Smalley, J. F.; Sachs, S. B.; Chidsey, C. E. D.; Dudek, S. P.; Sikes, H. D.; Creager, S. E.; Yu, C. J.; Feldberg, S. W.; Newton, M. D. Interfacial Electron-Transfer Kinetics of Ferrocene through Oligophenyleneethynylene Bridges Attached to Gold Electrodes as Constituents of Self-Assembled Monolayers: Observation of a Nonmonotonic Distance Dependence. *J. Am. Chem. Soc.* **2004**, *126* (44), 14620−14630.

(50) Smalley, J. F.; Finklea, H. O.; Chidsey, C. E. D.; Linford, M. R.; Creager, S. E.; Ferraris, J. P.; Chalfant, K.; Zawodzinsk, T.; Feldberg, S. W.; Newton, M. D. Heterogeneous Electron-Transfer Kinetics for Ruthenium and Ferrocene Redox Moieties through Alkanethiol Monolayers on Gold. *J. Am. Chem. Soc.* **2003**, *125* (7), 2004−2013.

(51) Seto, K.; Nakayama, T.; Uno, B. Formal Redox Potentials of Organic Molecules in Ionic Liquids on the Basis of Quaternary Nitrogen Cations as Adiabatic Electron Affinities. *J. Phys. Chem. B* **2013**, *117* (37), 10834−10845.

(52) Randviir, E. P. A Cross Examination of Electron Transfer Rate Constants for Carbon Screen-Printed Electrodes Using Electrochemical Impedance Spectroscopy and Cyclic Voltammetry. *Electrochim. Acta* **2018**, *286*, 179−186.

(53) Radtke, V.; Priester, D.; Heering, A.; Müller, C.; Koslowski, T.; Leito, I.; Krossing, I. The Unified Redox Scale for All Solvents: Consistency and Gibbs Transfer Energies of Electrolytes from Their Constituent Single Ions. *Chem.-Eur. J.* **2023**, *29* (46), No. e202300609.

(54) Qu, X.; Persson, K. A. Toward Accurate Modeling of the Effect of Ion-Pair Formation on Solute Redox Potential. *J. Chem. Theory Comput.* **2016**, *12* (9), 4501−4508.

(55) Pavlishchuk, V. V.; Addison, A. W. Conversion constants for redox potentials measured versus different reference electrodes in acetonitrile solutions at 25 °C. *Inorg. Chim. Acta* **2000**, *298* (1), 97−102.

(56) Nikitina, V. A.; Kislenko, S. A.; Nazmutdinov, R. R.; Bronshtein, M. D.; Tsirlina, G. A. Ferrocene/Ferrocenium Redox Couple at Au(111)/Ionic Liquid and Au(111)/Acetonitrile Interfaces: A Molecular-Level View at the Elementary Act. *J. Phys. Chem. C* **2014**, *118* (12), 6151−6164.

(57) Namazian, M.; Lin, C. Y.; Coote, M. L. Benchmark Calculations of Absolute Reduction Potential of Ferricinium/Ferrocene Couple in Nonaqueous Solutions. *J. Chem. Theory Comput.* **2010**, *6* (9), 2721−2725.

(58) Mugisa, J.; Chukwu, R.; Brogioli, D.; La Mantia, F. Effect of Ion-Paring on the Kinetics of Redox Systems with Concentrated Supporting Electrolyte. *Electrochim. Acta* **2024**, *473*, 143473.

(59) Makoś, M. Z.; Gurunathan, P. K.; Raugei, S.; Kowalski, K.; Glezakou, V.-A.; Rousseau, R. Modeling Absolute Redox Potentials of Ferrocene in the Condensed Phase. *J. Phys. Chem. Lett.* **2022**, *13* (42), 10005−10010.

(60) Kim, D. Y.; Yang, J. C.; Kim, H. W.; Swain, G. M. Heterogeneous Electron-Transfer Rate Constants for Ferrocene and Ferrocene Carboxylic Acid at Boron-Doped Diamond Electrodes in a Room Temperature Ionic Liquid. *Electrochim. Acta* **2013**, *94*, 49−56.

(61) Aranzaes, J. R.; Daniel, M.-C.; Astruc, D. Metallocenes as References for the Determination of Redox Potentials by Cyclic Voltammetry Permethylated Iron and Cobalt Sandwich Complexes, Inhibition by Polyamine Dendrimers, and the Role of Hydroxy-Containing Ferrocenes. *Can. J. Chem.* **2006**, *84* (2), 288−299.

(62) Bao, D.; Millare, B.; Xia, W.; Steyer, B. G.; Gerasimenko, A. A.; Ferreira, A.; Contreras, A.; Vullev, V. I. Electrochemical Oxidation of Ferrocene: A Strong Dependence on the Concentration of the Supporting Electrolyte for Nonpolar Solvents. *J. Phys. Chem. A* **2009**, *113* (7), 1259−1267.

(63) Chatterley, A. S.; Lackner, F.; Pemmaraju, C. D.; Neumark, D. M.; Leone, S. R.; Gessner, O. Dissociation Dynamics and Electronic Structures of Highly Excited Ferrocenium Ions Studied by Femtosecond XUV Absorption Spectroscopy. *J. Phys. Chem. A* **2016**, *120* (48), 9509−9518.

(64) Flores-Leonar, M. M.; Moreno-Esparza, R.; Ugalde-Saldívar, V. M.; Amador-Bedolla, C. Further Insights in DFT Calculations of Redox Potential for Iron Complexes: The Ferrocenium/Ferrocene System. *Computational and Theoretical Chemistry* **2017**, *1099*, 167−173.

(65) Takano, Y.; Houk, K. N. Benchmarking the Conductor-like Polarizable Continuum Model (CPCM) for Aqueous Solvation Free Energies of Neutral and Ionic Organic Molecules. *J. Chem. Theory Comput.* **2005**, *1* (1), 70−77.

(66) Zhao, Y.; Truhlar, D. G. The M06 Suite of Density Functionals for Main Group Thermochemistry, Thermochemical Kinetics, Noncovalent Interactions, Excited States, and Transition Elements: Two New Functionals and Systematic Testing of Four M06-Class Functionals and 12 Other Functionals. *Theor. Chem. Acc.* **2008**, *120* (1−3), 215−241.

(67) Becke, A. D. Density-Functional Exchange-Energy Approximation with Correct Asymptotic Behavior. *Phys. Rev. A* **1988**, *38* (6), 3098−3100.

(68) Lippert, B. G.; Hutter, J.; Parrinello, M. A Hybrid Gaussian and Plane Wave Density Functional Scheme. *Mol. Phys.* **1997**, *92* (3), 477−488.

(69) Schiller, C.; Sieh, D.; Lindenmaier, N.; Stephan, M.; Junker, N.; Reijerse, E.; Granovsky, A. A.; Burger, P. Cleavage of an Aromatic C-C Bond in Ferrocene by Insertion of an Iridium Nitrido Nitrogen Atom. *J. Am. Chem. Soc.* **2023**, *145* (20), 11392−11401.

(70) Chamkin, A. A.; Serkova, E. S. DFT, DLPNO-CCSD(T), and NEVPT2 Benchmark Study of the Reaction between Ferrocenium and Trimethylphosphine. *J. Comput. Chem.* **2020**, *41* (28), 2388−2397.

(71) Trasatti, S. The Absolute Electrode Potential: An Explanatory Note (Recommendations 1986). *Pure Appl. Chem.* **1986**, *58* (7), 955−966.

(72) Busch, M.; Ahlberg, E.; Laasonen, K. From Absolute Potentials to a Generalized Computational Standard Hydrogen Electrode for Aqueous and Non-Aqueous Solvents. *Phys. Chem. Chem. Phys.* **2021**, *23* (20), 11727−11737.

(73) Busch, M.; Ahlberg, E.; Ahlberg, E.; Laasonen, K. How to Predict the pKa of Any Compound in Any Solvent. *ACS Omega* **2022**, *7* (20), 17369−17383.

(74) Busch, M.; Laasonen, K.; Ahlberg, E. Method for the Accurate Prediction of Electron Transfer Potentials Using an Effective Absolute Potential. *Phys. Chem. Chem. Phys.* **2020**, *22* (44), 25833−25840.

(75) Wang, H.; Zhu, H.-W.; Guo, R.-R.; Hu, Q.-L.; Zeng, S.; Lu, J.-X. Computational and Experimental Study on Electrocarboxylation of Benzalacetone. *Asian Journal of Organic Chemistry* **2017**, *6* (10), 1380−1384.

(76) Warburton, R. E.; Soudackov, A. V.; Hammes-Schiffer, S. Theoretical Modeling of Electrochemical Proton-Coupled Electron Transfer. *Chem. Rev.* **2022**, *122* (12), 10599−10650.

(77) Bard, A. J.; Faulkner, L. R. *Electrochemical Methods: Fundamentals and Applications*, 2nd ed.; Wiley, 2001.

(78) Parson, W. W. Reorganization Energies, Entropies, and Free Energy Surfaces for Electron Transfer. *J. Phys. Chem. B* **2021**, *125* (29), 7940−7945.

(79) Kodis, G.; Ertem, M. Z.; Newton, M. D.; Matyushov, D. V. Reorganization Energy of Electron Transfer in Ionic Liquids. *J. Phys. Chem. Lett.* **2022**, *13* (14), 3297−3303.

(80) Govind Rajan, A.; Carter, E. A. Microkinetic model for pH- and potential-dependent oxygen evolution during water splitting on Fe-doped β-NiOOH. *Energy Environ. Sci.* **2020**, *13* (12), 4962−4976.

(81) Zhang, L.; Huang, J. Understanding Surface Charge Effects in Electrocatalysis. Part I: Peroxodisulfate Reduction at Pt(111). *J. Phys. Chem. C* **2020**, *124* (31), 16951−16960.

(82) Hsu, C.-P. Reorganization Energies and Spectral Densities for Electron Transfer Problems in Charge Transport Materials. *Phys. Chem. Chem. Phys.* **2020**, *22* (38), 21630−21641.

(83) Lehmann, K.; Yurchenko, O.; Urban, G. Carbon Nanowalls for Oxygen Reduction Reaction in Bio Fuel Cells. *J. Phys.: Conf. Ser.* **2014**, *557* (1), 012008.

(84) Henstridge, M. C.; Laborda, E.; Compton, R. G. Asymmetric Marcus-Hush Model of Electron Transfer Kinetics: Application to the Voltammetry of Surface-Bound Redox Systems. *J. Electroanal. Chem.* **2012**, *674*, 90−96.

(85) Gosser, D. K. *Cyclic Voltammetry: Simulation and Analysis of Reaction Mechanisms*, 1st ed.; Wiley VCH: New York, N.Y., 1993.

(86) Brown, J. H. Development and Use of a Cyclic Voltammetry Simulator To Introduce Undergraduate Students to Electrochemical Simulations. *J. Chem. Educ.* **2015**, *92* (9), 1490−1496.

(87) Vasudevan, D.; Wendt, H. Electroreduction of Oxygen in Aprotic Media. *J. Electroanal. Chem.* **1995**, *392* (1−2), 69−74.

(88) Chiyindiko, E.; Conradie, J. An Electrochemical and Computational Chemistry Study of Substituted Benzophenones. *Electrochim. Acta* **2021**, *373*, 137894.

(89) Masnovi, J. M.; Seddon, E. A.; Kochi, J. K. Electron Transfer from Anthracenes. Comparison of Photoionization, Charge-Transfer Excitation and Electrochemical Oxidation. *Can. J. Chem.* **1984**, *62* (11), 2552−2559.

(90) Sioda, R. E. Electrolytic Oxidation of 9,10-Diphenylanthracene and Properties of Its Free Radical Cation and Anion. *J. Phys. Chem.* **1968**, *72* (7), 2322−2330.

(91) Kotani, H.; Ohkubo, K.; Fukuzumi, S. Photocatalytic Oxygenation of Anthracenes and Olefins with Dioxygen via Selective Radical Coupling Using 9-Mesityl-10-Methylacridinium Ion as an Effective Electron-Transfer Photocatalyst. *J. Am. Chem. Soc.* **2004**, *126* (49), 15999−16006.

(92) Zhu, X.; Huang, J.; Eikerling, M. Electrochemical CO2 Reduction at Silver from a Local Perspective. *ACS Catal.* **2021**, *11* (23), 14521−14532.

(93) Bohra, D.; Chaudhry, J. H.; Burdyny, T.; Pidko, E. A.; Smith, W. A. Modeling the Electrical Double Layer to Understand the Reaction Environment in a CO2 Electrocatalytic System. *Energy Environ. Sci.* **2019**, *12* (11), 3380−3389.

(94) Wang, B.; Li, C.; Xiangyu, J.; Zhu, T.; Zhang, J. Z. H. An Approach to Computing Solvent Reorganization Energy. *J. Chem. Theory Comput.* **2020**, *16* (10), 6513−6519.

(95) Zhuang, B.; Wang, Z.-G. Molecular-Based Theory for Electron-Transfer Reorganization Energy in Solvent Mixtures. *J. Phys. Chem. B* **2016**, *120* (26), 6373−6382.